*Journal of Sound and Vibration* (1993) **165**(2), 341–359

# AXIAL VIBRATIONS OF A STOCHASTIC ROD

C. S. MANOHAR AND A. J. KEANE

*Department of Engineering Science, University of Oxford, Parks Road, Oxford, OX1 3PJ, England*

(*Received* 7 *October* 1991, *and in final form* 12 *March* 1992)

The free and forced axial vibration of a rod with stochastically varying mass and stiffness properties is considered. Exact probabilistic descriptions of the response variables are shown to be obtainable for a highly idealized case. The probability distributions of the eigensolutions, Green function and input receptance function for this case are obtained. The usefulness of these results as benchmarks in the study of confidence limits of responses predicted by Statistical Energy Analysis (S.E.A.) is noted.

## 1. INTRODUCTION

A principal aim of Statistical Energy Analysis (S.E.A.) has been the analysis of vibrating systems as drawn from an ensemble of random systems; see the books by Lyon [1]. These ensembles are thought of as arising out of random fluctuations in the material, geometric and topological characteristics of the system under study. Consequently, the dynamic characteristics, such as natural frequencies, mode shapes and transfer functions, of either the system taken as a whole or of the individual component subsystems become stochastic in nature. Originally, effort was centered on establishing the mean values of the various responses being studied, but more recently higher order statistics have become of interest: i.e., the calculation of confidence estimates for the predicted averages. Potentially, this interest leads to a rigorous forced response analysis of the system, where the probability density function (pdf) of the response variables must be related to the random fluctuations in the properties of the system. This problem is evidently too complicated for a general analytical solution, and for most cases can be approached only through numerical methods based on Monte Carlo simulation techniques.

Monte Carlo techniques are quite good at predicting mean values but become increasingly poor as higher order statistics are surveyed. Even so, they must faithfully reproduce the required statistical variation in the ensemble being studied, the size of which fundamentally affects the accuracy of the results. Before an extensive program of such numerical simulations is undertaken for any given structural configuration, it is obviously desirable to establish benchmark results against which the simulation algorithm can be validated. The present work has been focused on obtaining just such a benchmark. An exact and fairly complete, probabilistic description of the response of an idealized random structural system is considered: specifically, the axial vibration of a fixed-fixed rod, the stiffness and mass properties of which vary randomly along its length has been studied. The pdf of the eigenvalues of the rod are determined by using a procedure proposed by Iyengar and Athreya [2], and developed further by Iyengar and Manohar [3] and Manohar and Iyengar [4]. For a specific combination of system parameters it has been shown in reference [3] that an exact expression for the pdf of the eigenvalues is obtainable. Although highly idealized, this result is developed further in the present study to determine the pdf of the



0022–460X/93/170341 + 19 $08.00/0

eigenfunctions, the Green function and the input receptance function. As such it provides a benchmark for other methods which deal with more physically realizable cases. In a future study these results will be incorporated into the "exact" formulations presented by Keane and Price [5] to determine the pdf of the energy flows in an assembly of two coupled rods.

## 2. EQUATIONS OF MOTION

The axial vibration of a viscously damped fixed–fixed rod is governed by

$$\frac{\partial}{\partial \tilde{x}}\left[A(\tilde{x})E(\tilde{x})\frac{\partial \tilde{y}}{\partial \tilde{x}}\right]=\rho(\tilde{x})\frac{\partial^2 \tilde{y}}{\partial t^2}+C(\tilde{x})\frac{\partial \tilde{y}}{\partial t}-\tilde{F}(\tilde{x},t), \qquad \tilde{y}(0,t)=0, \quad \tilde{y}(L,t)=0. \tag{1}$$

Here $A(\tilde{x})$ is the area of cross-section, $E(\tilde{x})$ is the Young's modulus of elasticity, $\rho(\tilde{x})$ is the mass density per unit length, $C(\tilde{x})$ is the coefficient of viscous damping, $\tilde{F}(\tilde{x}, t)$ is the external force acting on the rod and $L$ is the length of the rod. In the present study the quantities $A$, $E$ and $\rho$ are taken to vary randomly along the length of the rod $\tilde{x}$. The damping coefficient is assumed to be proportional to the mass process and hence this also varies randomly in space. The force $\tilde{F}(\tilde{x}, t)$ could be random in both $\tilde{x}$ and $t$ co-ordinates, but attention is focused in the present study on $\tilde{F}$ being a point harmonic/random force. By non-dimensionalizing both the dependent and independent variables with respect to the length of the rod and introducing the variables,

$$x=\tilde{x}/L, \qquad y=\tilde{y}/L, \qquad A(x)E(x)=A_0E_0[1+\gamma g(x)], \tag{2–4}$$

$$\rho(x)=\rho_0[1+\varepsilon f(x)], \qquad C(x)=\nu\rho_0[1+\varepsilon f(x)], \tag{5, 6}$$

$$\mu^2=\rho_0L^2/A_0E_0, \qquad \beta=\nu L^2/A_0E_0, \qquad F(x,t)=L\tilde{F}/A_0E_0, \tag{7–9}$$

the system of equations (1) can be recast as

$$\frac{\partial}{\partial x}\left\{[1+\gamma g(x)]\frac{\partial y}{\partial x}\right\}=\mu^2[1+\varepsilon f(x)]\frac{\partial^2 y}{\partial t^2}+\beta[1+\varepsilon f(x)]\frac{\partial y}{\partial t}-F(x,t), \tag{10}$$

$$y(0,t)=0, \quad y(1,t)=0.$$

Here the functions $g(x)$ and $f(x)$ are taken to be jointly stationary random processes which are bounded in a mean square sense. Clearly, the quantities $[1+\gamma g(x)]$ and $[1+\varepsilon f(x)]$ must be strictly positive for all values of $x$.

## 3. RANDOM EIGENVALUES

The study of the eigensolutions of equation (10) involves the solution of the stochastic boundary value problem given by

$$\frac{\mathrm{d}}{\mathrm{d}x}\left\{[1+\gamma g(x)]\frac{\mathrm{d}Y}{\mathrm{d}x}\right\}+\lambda^2[1+\varepsilon f(x)]Y=0, \qquad Y(0)=0, \qquad Y(1)=0. \tag{11, 12}$$

Here the eigenvalue parameter $\lambda$ is a random variable and the solution $Y(x)$ is a random process. A complete solution of equations (11, 12) involves the determination of the joint probability density function of the eigenvalues and the eigenfunctions. A general solution of this problem does not currently appear to be possible. However, for specific models for $f(x)$ and $g(x)$, solutions for the pdf of the eigenvalues can be obtained by using the

procedure outlined in references [2–4]. This procedure can be briefly summarized as follows.

For an *arbitrarily* assigned value of $\lambda$, let $Y^*(x, \lambda)$ be the solution of equation (11) together with the *initial* conditions

$$Y^*(0, \lambda) = 0, \qquad (\mathrm{d}Y^*/\mathrm{d}x)(1, \lambda) = 1. \tag{13}$$

Let $Z_n(\lambda)$ denote the $n$th zero of $Y^*(x, \lambda)$. It is known from the Sturm–Liouville theory of ordinary differential equation that the $Z_n(\lambda)$ are non-increasing in $\lambda$; see, for example, the book by Birkhoff and Rota [6]. Note that the $\lambda$'s, which are the eigenvalues of the equations (11) and (12), satisfy the relation

$$Z_n(\lambda) = 1. \tag{14}$$

Thus, the problem of characterizing the eigenvalues of equations (11) and (12) can be posed in terms of the study of $Z_n(\lambda)$. To facilitate this study, it is useful to introduce a pair of amplitude and phase functions through the co-ordinate transformation

$$Y^*(x, \lambda) = r(x) \sin \phi(x). \qquad [1 + \gamma g(x)]\, \mathrm{d}Y/\mathrm{d}x = r(x)\lambda \cos \phi(x). \tag{15, 16}$$

The governing equations for $r(x)$ and $\phi(x)$ can then be shown to be given by

$$\frac{\mathrm{d}r}{\mathrm{d}x} = \frac{\lambda r}{2}\left[\frac{1}{(1+\gamma g)} - (1+\varepsilon f)\right] \sin 2\phi, \qquad \frac{\mathrm{d}\phi}{\mathrm{d}x} = \lambda\left[\frac{\cos^2\phi}{(1+\gamma g)} + (1+\varepsilon f)\sin^2\phi\right], \tag{17, 18}$$

together with the initial conditions

$$r(0) = [1 + \gamma g(0)]/\lambda, \qquad \phi(0) = 0. \tag{19, 20}$$

It is observed from the above that $\phi(x, \lambda)$ is non-decreasing in $x$ and also that

$$\phi[Z_n(\lambda), \lambda] = n\pi. \tag{21}$$

Since $\phi(x)$ is non-decreasing in $x$ it follows that

$$P[Z_n(\lambda) \leqslant x] = P[\phi(Z_n(\lambda) \leqslant \phi(x, \lambda)] = P[n\pi \leqslant \phi(x, \lambda)]. \tag{22}$$

Furthermore, $Z_n(\lambda)$ is non-increasing in $\lambda$ and hence

$$P[\lambda_n \leqslant \lambda] = P[Z_n(\lambda) \leqslant 1] = P[n\pi \leqslant \phi(1, \lambda)]. \tag{23}$$

Thus, in order to find the pdf of $\lambda_n$, equation (18) must be solved together with the initial condition (20), for every value of $\lambda$; also the pdf of $\phi(x, \lambda)$ at $x = 1$ must be obtained. When $f(x)$ and $g(x)$ arise as stationary, broadband random processes it is possible to obtain acceptable approximations to the pdf of the eigenvalues by using Markov process theory [3, 4]. A discussion of this aspect is not pursued here but, instead, a special case which is amenable to an exact analytical treatment is considered.

## 4. A SPECIAL CASE

It can be seen from equations (17) and (18) that when $f(x)$ and $g(x)$ are such that

$$1 + \varepsilon f(x) = 1/[1 + \gamma g(x)], \tag{24}$$

the problem is significantly simplified. In this case

$$\phi(x) = \lambda x + \varepsilon\lambda \int_0^x f(s)\,\mathrm{d}s, \qquad r(x) = r(0), \tag{25, 26}$$

and hence

$$Y^*(x, \lambda) = r(0) \sin\left[\lambda x + \varepsilon\lambda \int_0^x f(s)\,\mathrm{d}s\right]. \tag{27}$$

The expression for the eigenfunctions $Y_n(x)$ and eigenvalues $\lambda_n$ can then be obtained by using the condition $Y^*(1, \lambda) = 0$. This leads to

$$Y_n(x) = \sin\left[\lambda_n\left(x + \varepsilon \int_0^x f(s)\,\mathrm{d}s\right)\right], \qquad \lambda_n = n\pi \Big/ \left[1 + \varepsilon \int_0^1 f(s)\,\mathrm{d}s\right]. \tag{28, 29}$$

Here the amplitude of the eigenfunctions has been normalized to unity. This results in no loss of generality since $r(x)$ as given by equation (26) is independent of $x$. Furthermore, it is of interest to note that the eigenfunctions satisfy, with probability one, the orthogonality condition

$$\int_0^1 Y_n(x)\, Y_k(x)[1 + \varepsilon f(x)]\,\mathrm{d}x = \left[1 + \varepsilon \int_0^1 f(s)\,\mathrm{d}s\right]\delta_{nk}/2, \tag{30}$$

where $\delta_{nk}$ is the Kronecker delta function. Once the probabilistic description of the process $f(x)$ is available, the pdf of the eigenvalues and the eigenfunctions can easily be determined

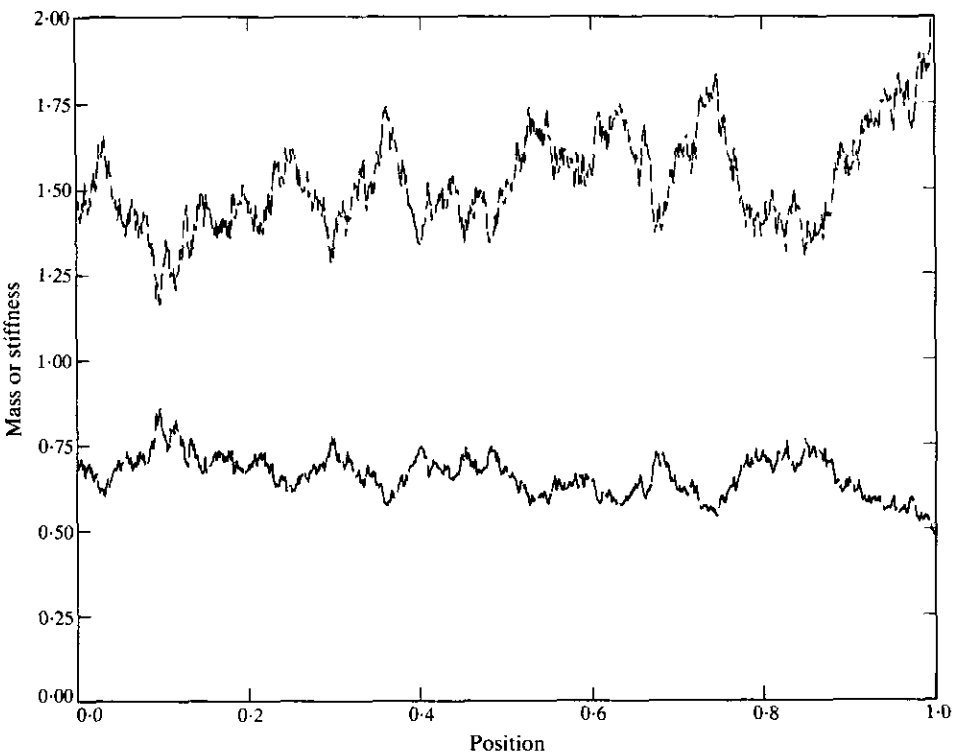


Figure 1. Example realizations of mass and stiffness processes: – – –, mass,: — —, stiffness.

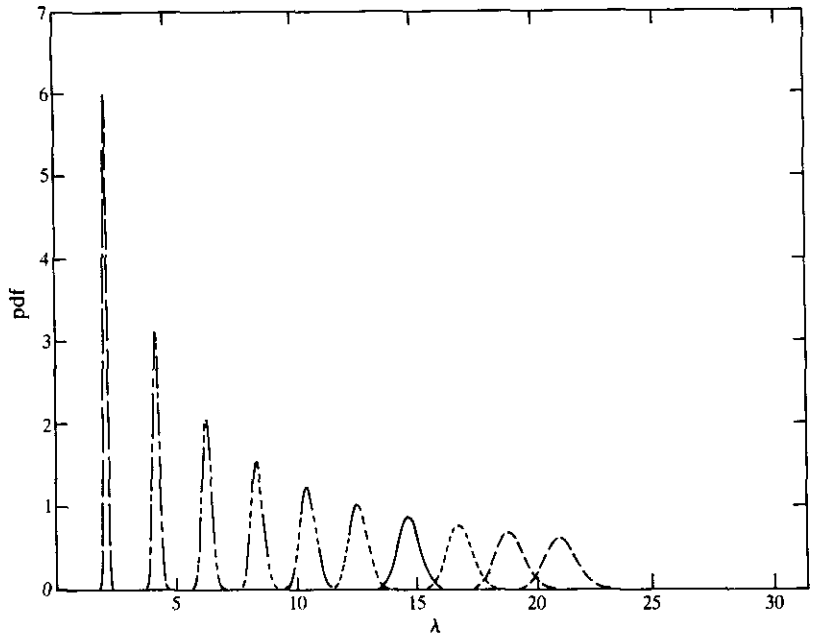


Figure 2. pdf of eigenvalues: — —, $n=1$; — · —, $n=2$; — · · —, $n=3$; — · · · —, $n=4$; — · · · · —, $n=5$; — · · · · · —, $n=6$; ——, $n=7$; - - - - -, $n=8$; - - -, $n=9$; — — —, $n=10$.

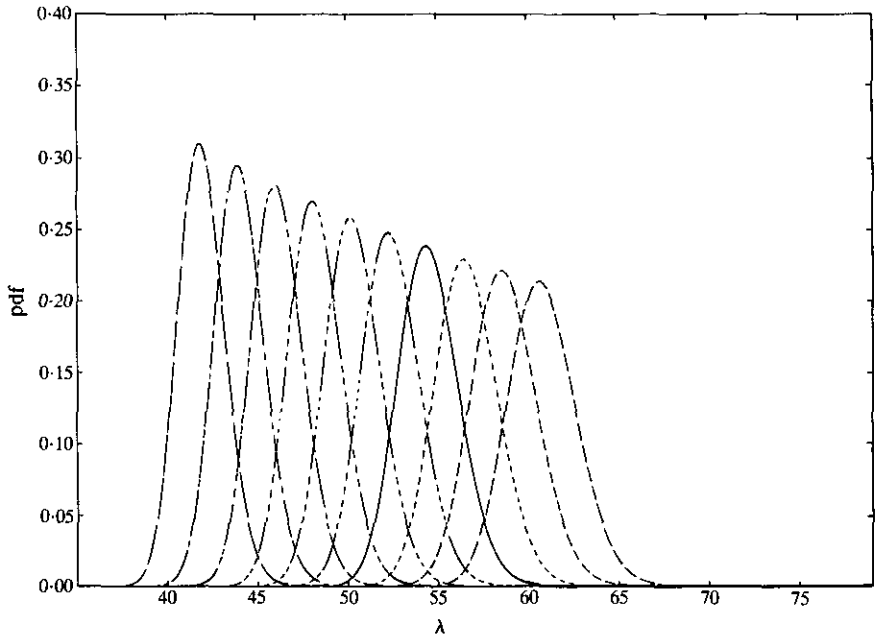


Figure 3. pdf of eigenvalues: — —, $n=20$; — · —, $n=21$; — · · —, $n=22$; — · · · —, $n=23$; — · · · · —, $n=24$; — · · · · · —, $n=25$; ——, $n=26$; - - - - -, $n=27$; - - -, $n=28$; — — —, $n=29$.

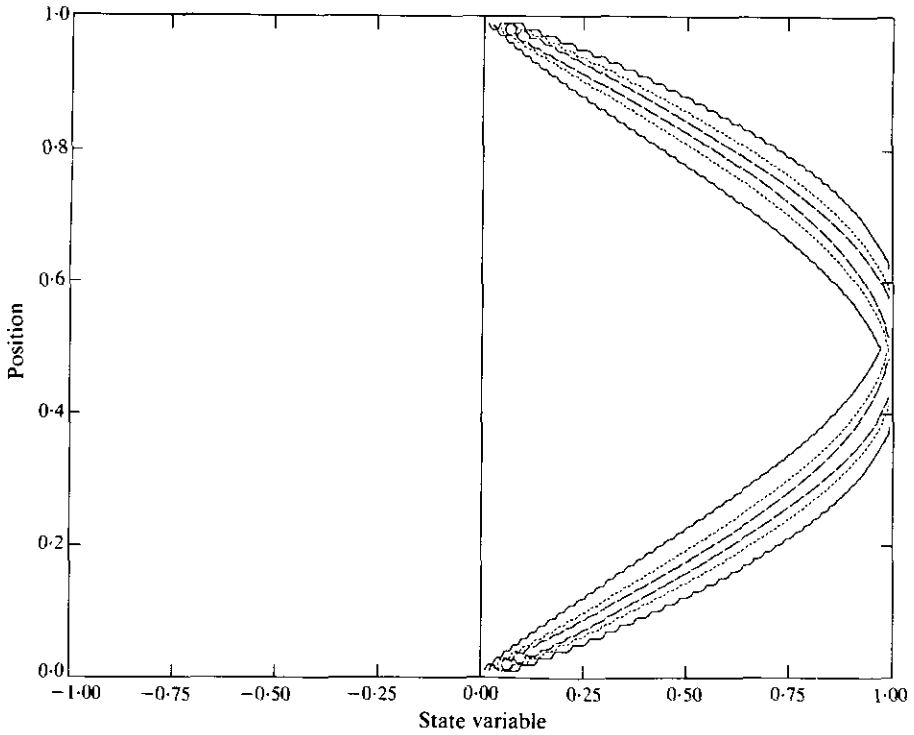


Figure 4. Contours for pdf of first eigenfunction: ——, 1·0E-04; - - - - -, 1·0; – – –, 10·0.

by using the rules of transformation of random variables. In the present study, for the sake of mathematical expediency, the process $f(x)$ is taken to be a stationary Gaussian random process modelled as

$$f(x) = m_f + \sigma_f \zeta(x). \tag{31}$$

Here $\zeta(x)$ is a Gaussian random process with zero mean and an autocorrelation function given by

$$R_\zeta(x_1, x_2) = \exp[-\alpha|x_1 - x_2|]. \tag{32}$$

It must be noted that as a consequence of modelling $f(x)$ as a Gaussian random process the stipulation that the mass process $\rho(x)$ is strictly positive is violated, albeit with a possibly low probability. In the same sense, the stiffness and damping processes also could become negative. Strictly speaking, this is not acceptable; however, for $(m_f/\sigma_f) \geqslant 3$ it is expected that this limitation is not crucial. Equations (28) and (29) together with the model for $f(x)$ given in equation (31) enable one to determine the pdf of any desired eigensolution. It is useful at this stage to introduce the notation

$$Q(x) = \int_0^x \zeta(s)\, \mathrm{d}s, \tag{33}$$

Clearly, $Q(x)$ is also a Gaussian process with zero mean and variance given by

$$\sigma_x^2 = \int_0^x \int_0^x R_\zeta(x_1, x_2)\, \mathrm{d}x_1\, \mathrm{d}x_2. \tag{34}$$

The pdf of the $n$th eigenvalue and the $n$th eigenfunction can be shown to be given, respectively, by

$$p_n(\lambda)=\frac{n\pi}{\varepsilon\sigma_f\sigma_1\lambda^2\sqrt{(2\pi)}}\exp\left[\frac{-1}{2\sigma_1^2}\left\{\frac{n\pi}{\varepsilon\sigma_f\lambda}-\frac{1+\varepsilon m_f}{\varepsilon\sigma_f}\right\}^2\right], \tag{35}$$

$$p_n(y,x)=\sum_{m=-\infty}^{+\infty}\frac{\alpha_1\alpha_3}{2\alpha_2}\sqrt{\frac{n}{\alpha_2}}\exp\left[-\alpha_4+\frac{\alpha_3^2}{4\alpha_2}\right], \tag{36}$$

$$\alpha_1=\frac{1}{bd\sqrt{(1-y^2)}2\pi\sigma_1\sigma_x\sqrt{(1-\sigma_{1x}^2)}}, \tag{37}$$

$$\alpha_2=\left[\frac{(\sin^{-1}y+2m\pi)^2}{\sigma_x^2b^2}+\frac{1}{d^2\sigma_1^2}-\frac{2\sigma_{1x}(\sin^{-1}y+2m\pi)}{\sigma_1\sigma_xbd}\right]\Big/2(1-\sigma_{1x}^2), \tag{38}$$

$$\alpha_3=-\left[\frac{-2a(\sin^{-1}y+2m\pi)}{\sigma_x^2b^2}-\frac{2c}{d^2\sigma_1^2}+\frac{2\sigma_{1x}a}{\alpha_1\sigma_xbd}+\frac{2\sigma_{1x}c(\sin^{-1}y+2m\pi)}{\sigma_1\sigma_xbd}\right]\Big/2(1-\sigma_{1x}^2), \tag{39}$$

$$\alpha_4=\left[\frac{a^2}{\sigma_x^2b^2}+\frac{c^2}{d^2\sigma_1^2}-\frac{2\sigma_{1x}ac}{\sigma_x\sigma_1bd}\right]\Big/2(1-\sigma_{1x}^2), \tag{40}$$

$$\sigma_{1x}=\left[\int_0^1\int_0^x R_\zeta(x_1x_2)\,dx_1\,dx_2\right]\Big/\sigma_1\sigma_x, \tag{41}$$

$$\sigma_1^2=\int_0^1\int_0^1 R_\zeta(x_1x_2)\,dx_1\,dx_2, \qquad a=n\pi x+n\pi x\varepsilon m_f, \tag{42, 43}$$

$$b=n\pi\varepsilon\sigma_f, \qquad c=1+\varepsilon m_f, \qquad d=\varepsilon\sigma_f. \tag{44–46}$$

It may also be noted that the derivation of the joint pdf between $\lambda_n$, $Y_n(x_1)$ and $Y_k(x_2)$ is fairly straightforward. However, the relevant expressions are quite complicated, and are therefore not presented here.

## 5. GREEN FUNCTION

The Green function denoted by $G(x, \xi, t, \tau)$ is defined as the solution of equation (10) when $F(x, t)=\delta(x-\xi)\,\delta(t-\tau)$ In terms of the natural frequency and mode shapes of the system the Fourier transform of the Green function is given by

$$G(x,\xi,\omega)=\sum_{m=1}^{\infty}\frac{2Y_n(x)Y_n(\xi)H_n(j\omega)}{\mu^2[1+\varepsilon\int_0^1 f(s)\,ds]}. \tag{47}$$

Here $Y_n(x)$ is the $n$th eigenfunction and $H_n(j\omega)$ is the complex frequency response function of the $n$th mode. When the eigensolutions of the system are random functions it is clear that the Green function is also random in nature and it is of interest to determine the pdf of this function. A general solution is again not available, but for the special case considered in the previous section, solutions can still be obtained.

From a study of equations (28), (29) and (47) it becomes apparent that for fixed values of $x$ and $\xi$ the quantity $G(x, \xi, \omega)$ is a function of three random variables; namely, $Q(x)$, $Q(\xi)$ and $Q(1)$. In the present study these random variables are taken to be jointly Gaussian. It may be noted that for fixed values of $x$ and $\xi$, $G(x, \xi, \omega)$ is a complex random

variable, and hence a complete description of this random variable would require the joint pdf between the real and imaginary parts. The highly non-linear nature of the transformation involved rules out the possibility of applying the standard method of finding the pdf of this function of random variables based on the inverse of the function. Alternatively, one can use the characteristic function method to determine the pdf of the transformed random variable. Thus, for instance, if one is interested in the amplitude of the Green function defined as

$$A(x, \xi, \omega) = \sqrt{\{\mathrm{Re}\,[G(x, \xi, \omega)]\}^2 + \{\mathrm{Im}\,[G(x, \xi. \omega)]\}^2}, \tag{48}$$

one can first find the characteristic function of $A$ using

$$\Phi_A(\Omega, x, \xi, \omega) = \langle \exp\,[\mathrm{j}\Omega A(x, \xi, \omega)] \rangle. \tag{49}$$

Here $\langle \cdot \rangle$ denotes the expectation operator. The pdf of $A$ can then be determined through the inverse Fourier transform, defined by

$$p_A(a, x, \xi, \omega) = \frac{1}{2\pi} \int_{-\infty}^{\infty} \Phi_A(\Omega, x, \xi, \omega) \exp\,(-\mathrm{j}\Omega a)\, \mathrm{d}\Omega. \tag{50}$$

In fact, this procedure for finding the pdf can be shown to be equivalent to using the identity

$$p_A(a, x, \xi, \omega) = \lim_{\Omega_c \to \infty} \left[\frac{1}{\pi}\right] \left\langle \frac{\sin\,\{\Omega_c[a - A(x, \xi, \omega)]\}}{\{a - A(x, \xi, \omega)\}} \right\rangle. \tag{51}$$

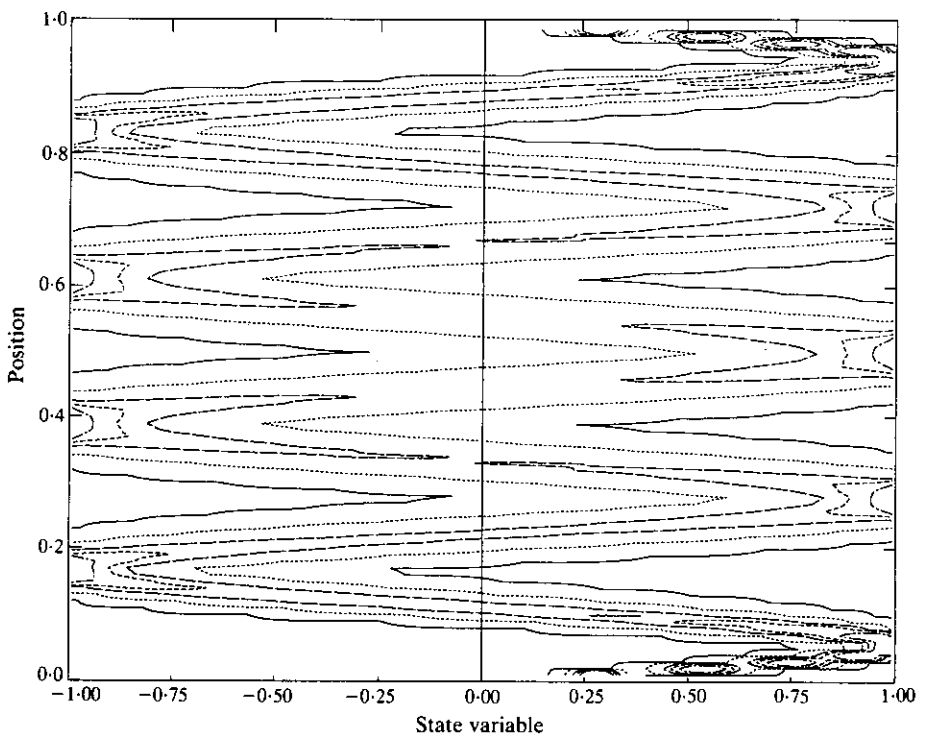


Figure 5. Contours for pdf of ninth eigenfunction: ——, 1·0E-04; - - - -, 0·1; – – –, 1.0; – – –, 2·0; — · —, 4·0.

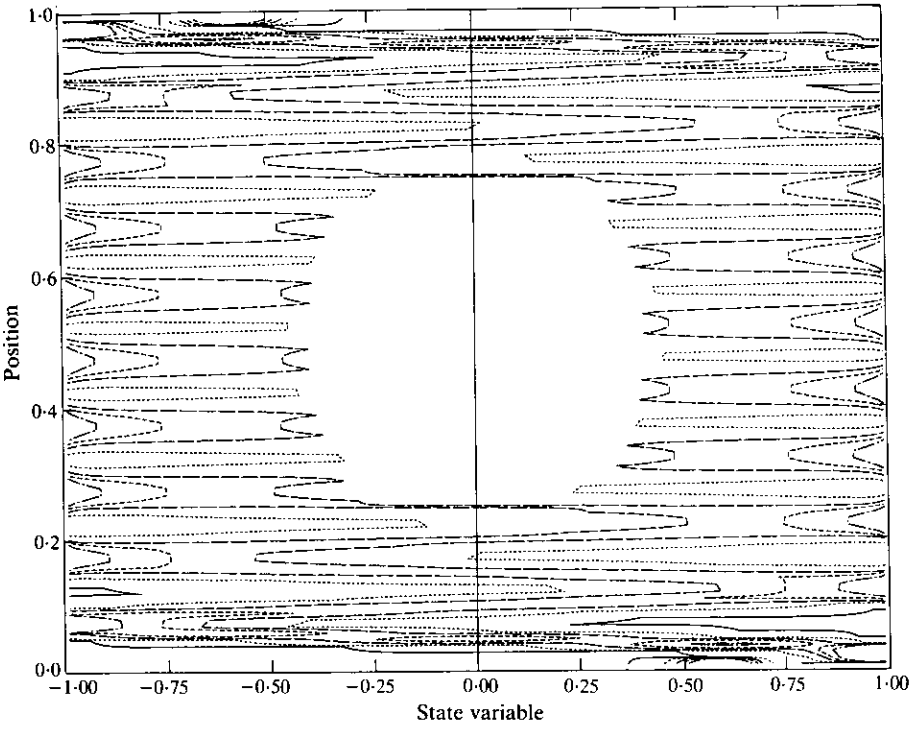


Figure 6. Contours for pdf of twentieth eigenfunction: ——, 1·0E-04; - - - - -, 0·1; — — —, 1.0; — — — —, 2·0; — · —, 4.0.

A proof of this simplification has been given by, for example, Pugachev [7]. It must be emphasized here that knowledge of the joint pdf of $Q(x)$, $Q(\xi)$ and $Q(1)$ would enable one to determine the expectation appearing in equations (49) and (51). However, evaluation of the integrals such as that in equation (51) in closed form is not feasible, and numerical techniques must be resorted to. The experience gained by the present authors in this direction has shown considerable numerical difficulties in evaluating such integrals and it has proven more advantageous to evaluate the equivalent probability *distribution* function (pdf). This entails an additional integration with respect to the state variable $a$ and upon this integration the expression for the distribution function becomes

$$P_A(a, x, \xi, \omega) = \lim_{\Omega_c \to \infty} \frac{1}{\pi} \langle \mathrm{Si}[\Omega_c a - \Omega_c A(x, \xi, \omega)] - \mathrm{Si}[-\Omega_c A(x, \xi, \omega)] \rangle. \tag{52}$$

Here $\mathrm{Si}(x)$ is the sine integral, defined as

$$\mathrm{Si}(x) = \int_0^x \frac{\sin s}{s} \, \mathrm{d}s. \tag{53}$$

This function can be easily computed by using the formulae listed by Abramowitz and Stegun [8]. It may be added that the joint probability distribution function of the real and the imaginary parts of the Green function can also be determined by following the steps outlined above.

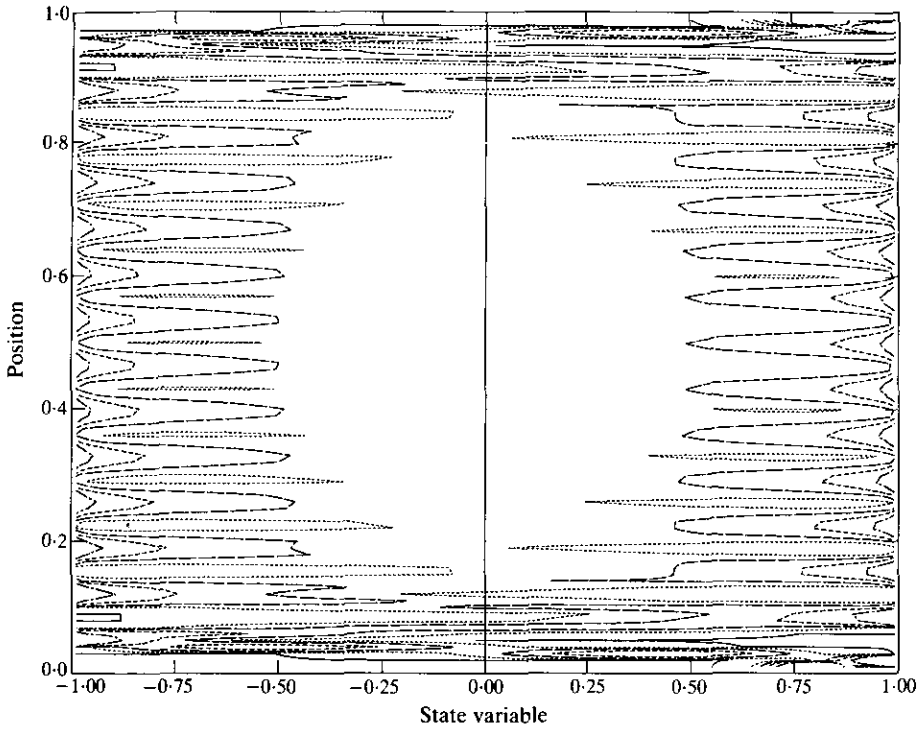


Figure 7. Contours for pdf of twenty-ninth eigenfunction: ——, 1·0E-04; - - - - -, 0·1; — —, 1·0; — — —, 2·0; — · —, 4·0.

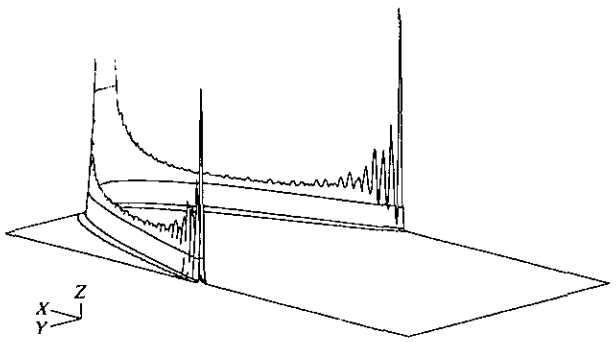


Figure 8. pdf of first eigenfunction.

## 6. INPUT RECEPTANCE

The total power input to the system when a force $F(x, t)$ acts on the system is given by

$$\Pi_{in}(t) = \int_0^L \dot{y}(x, t) F(x, t) F(x, t)\, \mathrm{d}x. \tag{54}$$

For the case of $F(x, t)$ being a unit white noise process acting at a point $x = x_0$, the average

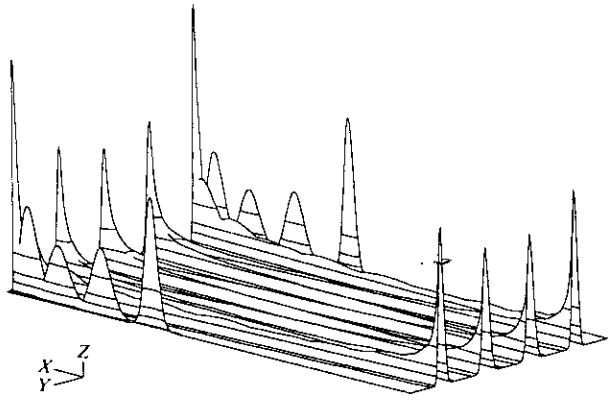


Figure 9. pdf of ninth eigenfunction.

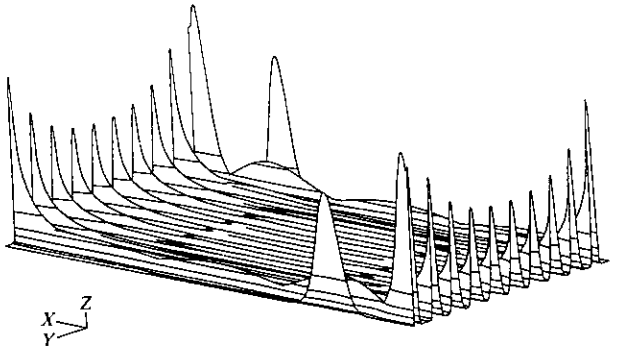


Figure 10. pdf of twentieth eigenfunction.

total power injected over long time periods can be written as

$$\lim_{t\to\infty} \langle \Pi_{in}(t) \rangle = \int_{-\infty}^{\infty} \Pi_{in}(x_0, \omega)\, \mathrm{d}\omega. \tag{55}$$

The function $\Pi_{in}(x_0, \omega)$ is termed the input receptance function, and can be shown to be given by

$$\Pi_{in}(x_0, \omega) = -\mathrm{j}\omega\ \mathrm{Im}\,[G(x_0, x_0, \omega)]. \tag{56}$$

This function is intimately related to various S.E.A. parameters and is of relevance to the present study; see, for example, the paper by Keane and Price [5]. When the system parameters are random quantities the pdf of this function is again of interest. For the special case discussed in section 4 this pdf can be obtained by using an approach similar to that already described in the previous section. It is clear from equation (47) that, for fixed values of $\omega$ and $x$, the input receptance is a function of two random variables; namely, $Q(x_0)$ and $Q(1)$. The probability distribution function of the input receptance function can thus be determined by using a relation similar to the one given in equation (52).

## 7. NUMERICAL RESULTS AND DISCUSSION

Numerical results have been obtained to illustrate the preceding theoretical analysis. A uniform rod having $L = 5{\cdot}186$ m, $A_0E_0 = 17{\cdot}85$ MN, $\rho_0 = 4{\cdot}156$ kg/m and $\nu = 80\ s^{-1}$ was randomized as per the model described in equations (24), (31) and (32). The parameters of the random process model for $f(x)$ were taken to be $\varepsilon = 0{\cdot}5$, $m_f = 1{\cdot}0$, $\sigma_f = 0{\cdot}3$ and $\alpha = 20{\cdot}0$. The variation of the mass and stiffness processes for one realization of an ensemble having these properties is illustrated in Figure 1.

The pdf is of the eigenvalues for modes 1–10 and 20–29 are shown in Figures 2 and 3, respectively. From equation (29) it can be deduced that the standard deviation of the $n$th eigenvalue is linearly proportional to $n$. Accordingly, from Figures 2 and 3 it can be seen that the spread in the pdf of the eigenvalues increases with increasing mode count. Consequently, in a probabilistic sense, there is a greater overlap of the eigenvalues in the higher frequency ranges. It is also of interest to note that there is an intrinsic regularity in the pdf of the eigenvalues in the sense that the pdf of the quantity $(\lambda_n/n)$ is invariant with respect to the changes in $n$. This property can be expected to be specific to the special case considered in this study and may not hold in general for axially vibrating random rods.

The pdf's of the first, ninth, twentieth and twenty-ninth eigenfunctions are presented as contour maps in Figures 4–7 as functions of non-dimensional position $x$. To facilitate the interpretation of these functions, three-dimensional views outlining the surface of the functions are shown in Figure 8–11. Notice that the "spiky" nature of these three-dimensional plots, particularly near the boundaries, arises from aliasing problems that occur during plotting, and such spikes are not present in the actual functions. The contours

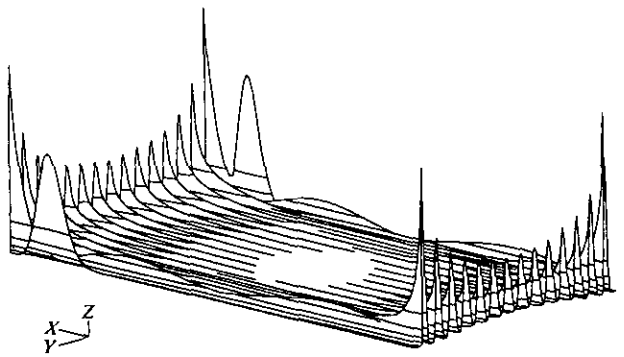


Figure 11. pdf of twenty-ninth eigenfunction.

shown in Figures 4–7 have also been marked in Figures 8–11 for comparison. Notice that here the infinite summation appearing in equation (36) has been carried out over the limits of $-50$ to 50, which ensures convergence. It is of interest to consider the variations in the structure of the pdf of the eigenfunctions along the length of the rod. Since at $x = 0$ and at $x = 1$ the displacements are zero, the pdf's degenerate at these points to Dirac's delta function centered at zero. This may be seen from the large peaks in the pdf near $x = 0$ and $x = 1$. It can further be observed from equation (28) and equations (36–46) that the eigenfunctions are bounded in $(-1, 1)$ and also that the pdf of the eigenfunctions has singularities at $y = \pm 1$. At the antinodes much of the probability is seen to be concentrated near one or other of these two extreme points. On the other hand, near the nodes, the eigenfunctions of lower modes are seen to have a Gaussian-like structure centered around a zero mean value, while for higher modes it tends to spread out and resemble an "arcsine"

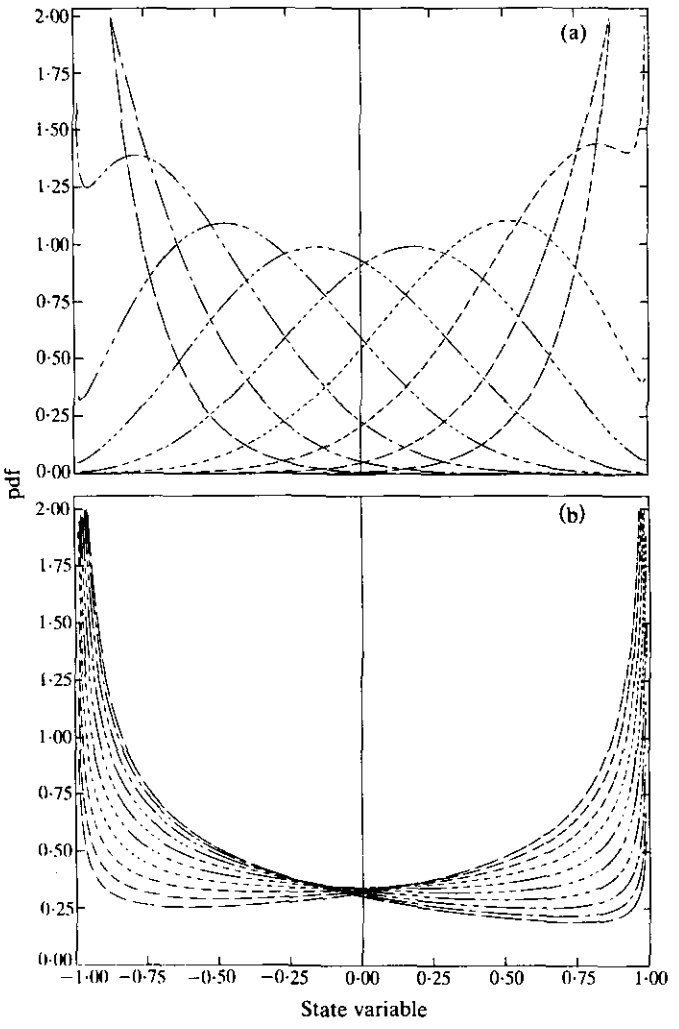


Figure 12. (a) pdf of ninth eigenfunction: — —, $x=0{\cdot}40$; — · —, $x=0{\cdot}41$; — · · —, $x=0{\cdot}42$; — · · · —, $x=0{\cdot}43$; — · · · · —, $x=0{\cdot}44$; — · · · · · —, $x=0{\cdot}45$; - - - - -, $x=0{\cdot}46$; — — —, $x=0{\cdot}47$; — — —, $x=0{\cdot}48$; — — -, $x=0{\cdot}49$. (b) pdf of twenty-ninth eigenfunction: — —, $x=0{\cdot}4000$; — · —, $x=0{\cdot}4025$; — · · —, $x=0{\cdot}4050$; — · · · —, $x=0{\cdot}4075$; — · · · · —, $x=0{\cdot}4100$; — · · · · · —, $x=0{\cdot}4125$; - - - - -, $x=0{\cdot}4150$; - - -, $x=0{\cdot}4175$; — —, $x=0{\cdot}4200$; — — —, $x=0{\cdot}4225$.

*type of function.* In the region between a node and antinode the pdf undergoes a continuous transformation between these two types of behaviour. This is illustrated in Figures 12(a) and 12(b), where cross-sections of the pdf of the ninth and twenty-ninth eigenfunctions are shown in a region spanning two successive antinodes. The variation in the shape of the pdf along the length of the rod is observed to be more pronounced for the eigenfunctions of the lower modes. This is perhaps because the higher modes have larger number of nodes and hence are constrained to oscillate a larger number of times. Consequently, they tend to have a more uniform structure for the pdf. As might be expected, the behaviour of the pdf of the eigenfunctions near the boundaries is invariably controlled by the boundary conditions which apply to all modes. It may be noted that it is possible to calculate the second order properties of the eigenfunctions such as their covariance functions, but this study is not pursued here.

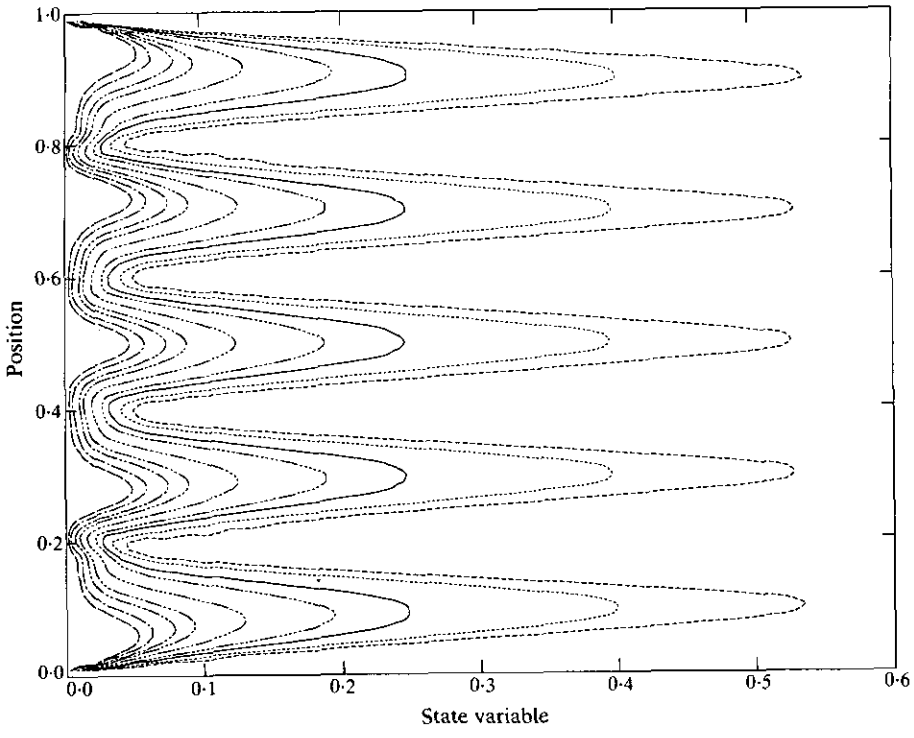


Figure 13. Contours for PDF of $|G(x, x, \omega)|$, $\omega = 4000$ rad/s: ——, 0·05; — · —, 0·1; — · · —, 0·2; — · · · —, 0·3; — · · · · —, 0·5; - - - - -, 0·7; ——, 0·8; · · · · ·, 0·9; – – –, 0·95.

The contours of the probability distribution function for the amplitude of the Green function for the case of $x = \xi$ and $\omega = 4000$ rad/s are plotted in Figure 13 as functions of position $x$. The corresponding functions for the case of $x \neq \xi$ are shown in Figure 14 for $\xi = 0{\cdot}2$, again as functions of $x$. For comparison the equivalent plots of the Green function amplitude for the deterministic case of $\sigma_f = 0$ are shown in Figures 15 and 16. The contours of the probability distribution of the input receptance function are presented in Figures 17 and 18 for $\omega = 4000$ rad/s and $\omega = 20\,000$ rad/s. The variations of the equivalent deterministic input receptance function for the case of $\sigma_f = 0$ at these driving frequencies are shown in Figures 19 and 20.

The values of $\omega = 4000$ rad/s and $\omega = 20\,000$ rad/s chosen here correspond, respectively, to $\lambda$ values of 10 and 50. From the plots of the pdf of the eigenvalues presented in Figures 2 and 3, it can be seen that the point $\lambda = 10$ lies between the fourth and fifth mode, while the point $\lambda = 50$ is centered around the twenty-fourth mode but is affected by all modes lying between the twenty-second and twenty-sixth: that is, these two frequencies lie near the centers of Figures 2 and 3 respectively. For the case of $\omega = 4000$ rad/s, the variations in the contours of the probability distribution of both the Green function amplitude and the input receptance broadly follow the pattern of variation of the corresponding deterministic curves. The fifth mode of vibration is seen to dominate the response. Clearly, the functions are non-stationary in nature. At higher frequencies the nature of these functions is affected by the greater overlap in the modes, and also by the tendency of the higher mode shapes to show rapid variations. These features are evident in Figure 18, where the contours of the probability distribution of the input receptance function for the case of $\omega = 20\,000$ rad/s are seen to be fairly constant in regions away from the boundaries, but to show wide fluctuations near them.

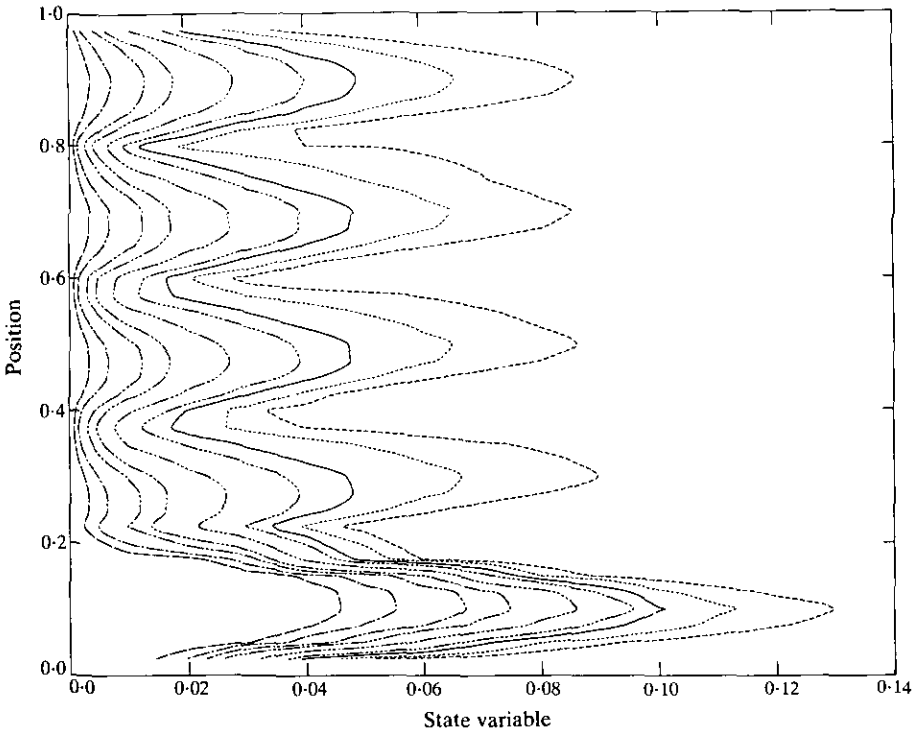


*Figure 14. Contours for PDF of $|G(x, \xi, \omega)|$, $\omega = 4000$ rad/s, $\xi = 0{\cdot}2$: ——, 0·05; — · —, 0·1; — · · —, 0·2; — · · · —, 0·3; — · · · · —, 0·5; - - - - -, 0·7; ——, 0·8; · · · · ·, 0·9; ——, 0·95.*

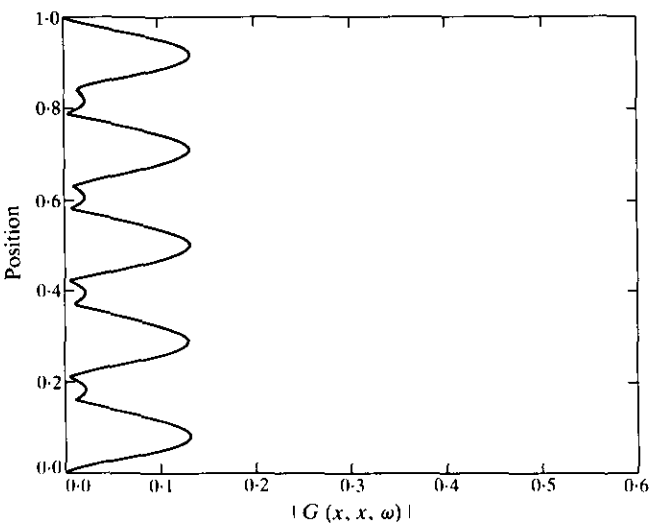


Figure 15. Deterministic $|G(x, x, \omega)|$, $\omega = 4000$ rad/s.

## 8. COMPUTATIONAL DETAILS

The probability distributions of the Green function and input receptance function have been obtained by using the formulation given in equation (52). The evaluation of the expectation appearing in this equation involves a multi-dimensional integration over infi-

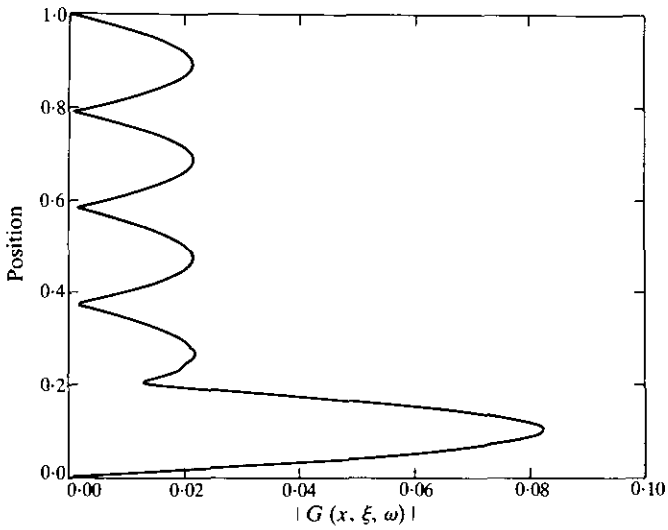


Figure 16. Deterministic $|G(x, \xi, \omega)|$, $\omega = 4000$ rad/s, $\xi = 0{\cdot}2$.

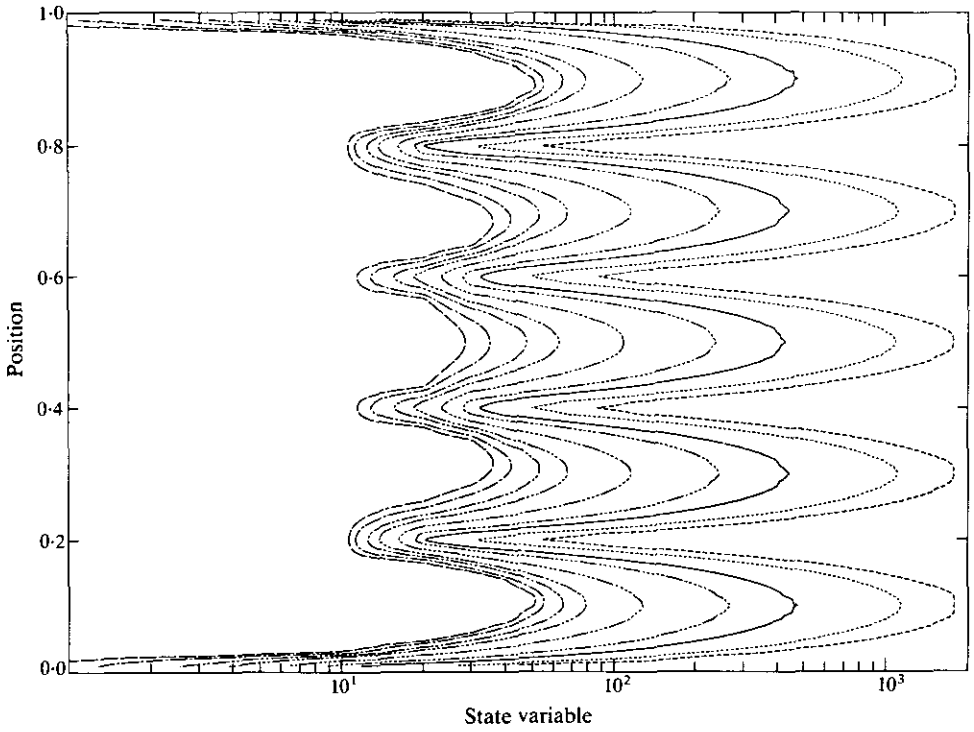


Figure 17. Contours for PDF of input power receptance function; $\omega = 4000$ rad/s: — —, 0·05; — · —, 0·1; — · · —, 0·2; — · · · —, 0·3; — · · · · —, 0·5; — · · · · · —, 0·7; ——, 0·8; - - - - -, 0·9; - - - -, 0·95.

nite limits with respect to a Gaussian distribution. The dimension of this integration is either two or three, depending on whether the case $x = \xi$ or $x \neq \xi$ is considered. Here a seventh order integration scheme has been employed to evaluate this integral. The limits of the integration are curtailed at five times the standard deviation away from the expected

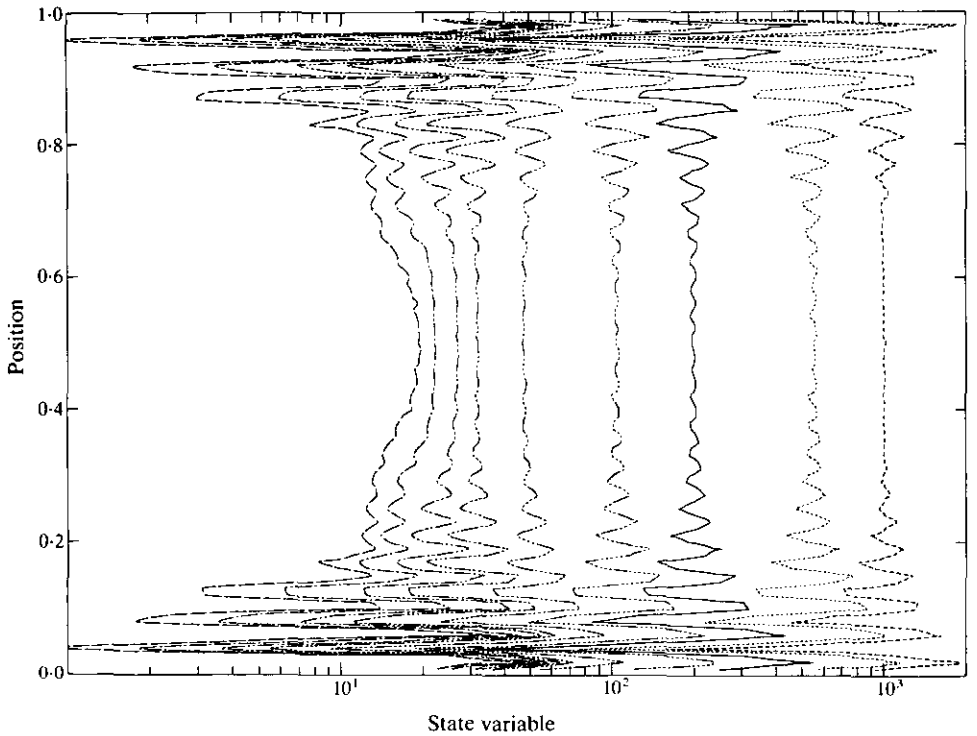


*Figure 18. Contours for PDF of input power receptance function; $\omega = 20\,000$ rad/s:* — —, 0·05; — · · —, 0·1; — · · —, 0·2; — · · · —, 0·3; — · · · · —, 0·5; — · · · · · —, 0·7; ——, 0·8; - - - - -, 0·9; - - - -, 0·95.

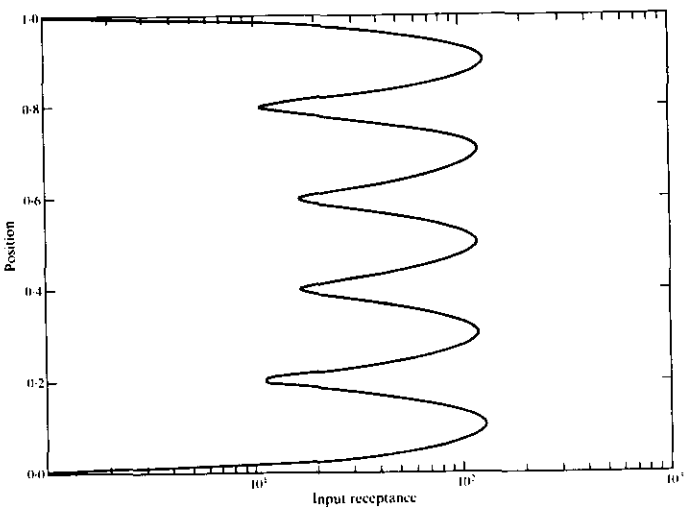


Figure 19. Deterministic input power receptance function; $\omega = 4000$ rad/s.

value of the Gaussian variate. The limiting operation with respect to the parameter $\Omega_c$ was found generally to converge at around $\Omega_c = 200$. The convergence of the probability distribution function of the input receptance function for the values of $x = 0{\cdot}2$ and $\omega = 4000$ rad/s with respect to the parameter $\Omega_c$ is shown in Figure 21. In this case the results

are seen to converge fairly quickly for $\Omega_c = 10{\cdot}0$. The terms to be retained in the summation over mode shapes appearing in the expression for the Green function clearly depend upon the driving frequency of interest. In these computations, for a given value of driving frequency, the nearest equivalent mode of the deterministic rod was first identified; the summation was then carried out from the first mode to that lying over 50 modes above this nearest mode. This is thought to guarantee convergence of the summations.

## 9. CONCLUSIONS

The axial vibration of a rod with randomly varying mass and stiffness properties has been considered. The probability density functions of the eigensolutions have been determined for a special case in which the mass and the stiffness processes bear a fixed relation to each other. These results are further used to evaluate the probability distribution functions of the rod Green function and its input receptance function. It has been shown for a specific example that the input receptance is only stationary with respect to position along the rod at driving frequencies significantly higher than the fifth natural frequency and then only for the central 30% of the rod's length. These results have been obtained by using analytical procedures and are exact in nature given the assumptions stated. It is intended in a future study to extend the results developed here to determine the probability distribution of the energy flows in an assembly of coupled rod systems. It is expected that such a study would afford useful insights into the problem of determining confidence limits for S.E.A. results.

The special case considered here is too limited in scope to be of any great practical importance. The results obtained can, however, serve the important function of providing benchmark results against which any alternative solution procedures with broader scope can be validated. It is precisely with this in mind that the present study has been undertaken. A general purpose Monte Carlo simulation algorithm is currently being developed by the present authors to study energy flows in multi-coupled rod configurations. The theoretical results developed in the present study will be used to validate this general purpose simulation algorithm. Specifically, they will enable checks to be made on the

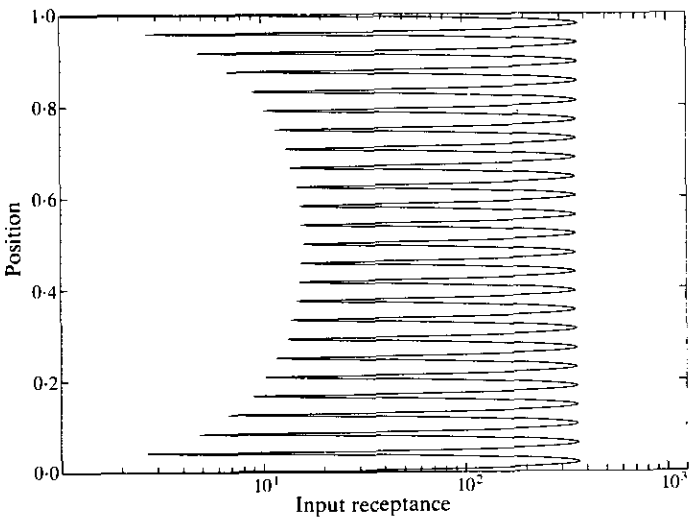


Figure 20. Deterministic input power receptance function: $\omega = 20\,000$ rad/s.

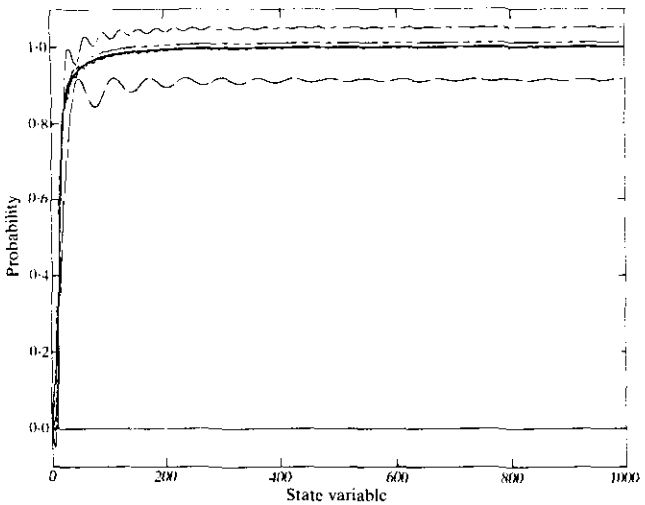


Figure 21. Convergence of PDF of input power receptance function with respect to parameter $\Omega_c$: — —, $\Omega_c = 0{\cdot}1$; — · —, $\Omega_c = 0{\cdot}2$; — · · —, $\Omega_c = 0{\cdot}4$; — · · · —, $\Omega_c = 0{\cdot}8$; — · · · · · —, $\Omega_c = 1{\cdot}6$; — · · · · · —, $\Omega_c = 3{\cdot}2$; ——, $\Omega_c = 6{\cdot}4$; - - - - -, $\Omega_c = 12{\cdot}8$; — — · —, $\Omega_c = 25{\cdot}6$, - - - -, $\Omega_c = 51{\cdot}2$.

modelling of the random processes used in the simulations and, more importantly, decisions on the ensemble sizes adopted to ensure suitable convergence.

## ACKNOWLEDGMENT

The support of the Department of Trade and Industry in carrying out this work is gratefully acknowledged.

## REFERENCES

1. R. H. LYON 1975 *Statistical Energy Analysis of Dynamical Systems: Theory and Applications.* Cambridge, Massachusetts: MIT Press.
2. R. N. IYENGAR and K. B. ATHREYA 1975 *Journal of the Indian Institute of Science* **57**, 185–191. A diffusion process approach to a random eigenvalue problem.
3. R. N. IYENGAR and C. S. MANOHAR 1989 *Transactions of the American Society of Mechanical Engineers, Journal of Applied Mechanics* **56**, 202–207. Probability distribution function of the eigenvalues of the random string equation.
4. C. S. MANOHAR and R. N. IYENGAR (to appear) *Probabilistic Engineering Mechanics.* Probability distribution of the eigenvalues of systems governed by the stochastic wave equation.
5. A. J. KEANE and W. G. PRICE 1990 *Proceedings of the Institute of Acoustics* **12**(1), 535–542 Exact power flow relationships between many multi-coupled, multi-modal sub-systems.
6. G. BIRKHOFF and G. C. ROTA 1969 *Ordinary Differential Equations.* New York: John Wiley.
7. V. S. PUGACHEV 1965 *Theory of Random Functions and its Application to Control Problems.* Oxford: Pergamon Press.
8. M. ABRAMOWITZ and I. A. STEGUN 1965 *Handbook of Mathematical Functions.* New York: Dover.